Polymer 128 (2017) 47–56

Contents lists available at ScienceDirect

Polymer

journal homepage: www.elsevier.com/locate/polymer

Cryogelation within cryogels: Silk fibroin scaffolds with single-, double- and triple-network structures

Berkant Yetiskin, Caner Akinci, Oguz Okay*

Istanbul Technical University, Department of Chemistry, 34469 Istanbul, Turkey

ARTICLE INFO

Article history:
Received 27 July 2017
Received in revised form
7 September 2017
Accepted 10 September 2017
Available online 11 September 2017

Keywords:
Silk fibroin
Cryogels
Scaffolds
Macroporous
Elasticity

ABSTRACT

Mechanically strong silk fibroin cryogels with two generations of pores were produced by carrying out the cryogelation reactions within the pores of the initial single-network (SN) fibroin cryogels. In this way, cryogels with interpenetrated and interconnected double- (DN), and triple-network (TN) structures were produced from fibroin solutions frozen at −18 °C in the presence of butanediol diglycidyl ether cross-linker and N,N,N′,N′-tetramethylethylenediamine as a pH regulator. Cryogel scaffolds formed at fibroin concentrations above 25 wt% exhibit a Young's modulus between 66 and 126 MPa, and sustain around 90% compressions under 87–240 MPa stresses. These values are the largest reported so far for fibroin scaffolds and hence the materials have promising applications in bone tissue engineering. We also show that the improvement in the mechanical performance of cryogels after multiple-networking is due to their increased content of fibroin network. Both DN and TN cryogels have two generations of interconnected macropores with diameters 20–30 μm and 3–9 μm. The size of both large and small pores could be adjusted by the relative amounts of fibroin in the network components.

1. Introduction

Silk fibroin gels and scaffolds are important materials for biomedical and biotechnological applications due to their good mechanical properties, biocompatibility, and controlled degradability [1–4]. Gelation of aqueous fibroin solutions mainly proceeds via self-assembly of fibroin molecules induced by hydrophobic associations to form intermolecular β-sheet crystallites acting as physical cross-link zones [5,6]. The conformational transition in fibroin from random coil to β-sheet structure leading to fibroin gelation can be induced by several triggers including pH [7–15], temperature [7,8], concentrations of fibroin [6,9,10], and additives such as cations [14–18], diepoxide cross-linkers [19], as well as vortexing [20], and electrical field [21–23].

In many application areas such as in bone tissue engineering, silk fibroin gels are required to possess a high mechanical strength and a 3D interconnected pore structure to provide a favorable microenvironment for cell attachment, infiltration, proliferation, and differentiation [4]. Several techniques have been used to prepare macroporous fibroin scaffolds including gas foaming, salt-leaching, electrospinning, and freeze-drying [24–34]. Silk fibroin scaffolds developed by these techniques exhibit Young's moduli between 10 kPa and 3 MPa. We recently introduced cryogelation technique to produce macroporous silk fibroin scaffolds exhibiting a very high Young's modulus (50 MPa) [35]. Although macroporous scaffolds in aqueous environments are usually brittle and rupture at a few tens percent of deformation, those derived from cryogels can completely be squeezed without any crack development [35]. As shown recently, silk fibroin cryogels are most promising candidates as a scaffold for bone regeneration [36].

The reason for the extraordinary mechanical performance of fibroin cryogels is their unusual formation history in an apparently frozen reaction system [35,37–39]. An aqueous fibroin solution containing a diepoxide cross-linker such as butanediol diglycidyl ether (BDDE) and N,N,N′,N′-tetramethylethylenediamine (TEMED) is first frozen at a subzero temperature, i.e., at −18 °C. As water freezes, fibroin, BDDE, and TEMED are expelled from the ice and they cryo-concentrate in the unfrozen micro-channels between the ice crystals. For instance, freezing of an aqueous 6 wt% fibroin solution at-18 °C results in a frozen system composed of 88% ice and the rest being a cryo-concentrated unfrozen solution containing 37 wt% fibroin [35]. To produce high-toughness scaffolds, all the reaction constituents should be cryo-concentrated before the onset of the cryogelation reactions [38]. For instance, freeze-drying

* Corresponding author.
E-mail address: okayo@itu.edu.tr (O. Okay).

http://dx.doi.org/10.1016/j.polymer.2017.09.023
0032-3861/

technique does not lead to mechanically strong scaffolds due to the formation of ice crystals in a gel rather than in the reaction solution. After conducting the cryogelation reactions in the unfrozen microdomains of the reaction system, cryogels with a macroporous structure form due to the presence of ice acting as template to form interconnected pores (Scheme 1a, b). The pore wall of fibroin cryogels is a dense gel because of the cryo-concentrated fibroin solution around the ice crystals leading to a high degree of toughness and complete squeezability [38,39].

The main idea leading to the present research is to produce cryogels with two generations of pores by carrying out the cryogelation reactions within the pores of a precursor cryogel, as schematically illustrated in Scheme 1b–d. Scaffolds having both large and small pores receive significant interest in tissue engineering due to the fact that the large pores of tens of micrometers in diameter are suitable for cell migration while smaller pores with a few micrometers are highly effective for nutrients and oxygen delivery [40–44]. To produce such scaffolds, the initial single-network fibroin cryogel scaffolds were first immersed in aqueous fibroin solutions containing BDDE and TEMED and then cryogelation reactions were conducted to produce fibroin cryogels with a double-network structure (Scheme 1b–d). By repeating this step, we were able to generate triple-network cryogels (Scheme 1e, f). In the following, the initial fibroin network is denoted as SN (single-network), and subsequent networks prepared within a previous network are designated as DN (double-network) and TN (triple-network). Thus, SN and DN fibroin scaffolds were used as precursors for the DN and TN cryogels, respectively.

We have to mention that DN cryogels based on synthetic polymers with pH- and temperature sensitivities have recently reported by Zhao et al. [45]. However, as will be discussed later, their mechanical strength is much lower than that of fibroin cryogels. Moreover, preparation of non-porous DN hydrogels is a well-known technique, first reported by Gong et al., in 2003, to improve the mechanical performance of chemically cross-linked brittle hydrogels [46,47]. The second-network of Gong's DN hydrogels is prepared in the gel phase while, in the present work, the second- and third-porous networks form within the pores of the precursor network thereby generating additional pores. As will be seen below, fibroin network components interpenetrate and interconnect each other resulting in the formation of water-insoluble SN, DN, and TN cryogels. Both the DNs and TNs have two generations of pores with diameters of 20–30 μm and 3–9 μm. The diameters of both large and small pores could be adjusted by the concentration of fibroin in the first and second gelation solution, respectively. Cryogel scaffolds formed at fibroin concentrations above 25 wt% exhibit a Young's modulus between 66 and 126 MPa, and sustain around 90% compressions under 87–240 MPa stresses. These values are the largest reported so far for fibroin scaffolds and suggest that the materials have promising applications in bone tissue engineering.

2. Experimental section

2.1. Materials

Butanediol diglycidyl ether (BDDE, Sigma-Aldrich), N,N,N′,N′-tetramethylethylenediamine (TEMED, Sigma-Aldrich), Na_2CO_3 (Merck), and LiBr (Merck) were used as received. *Bombyx mori* cocoons were purchased from Koza Birlik (Agriculture Sales Cooperative for Silk Cocoon, Bursa, Turkey). To separate silk fibroin from cocoons in the form of an aqueous solution, the method described by Kim et al. was utilized [7]. *Bombyx mori* cocoons were first boiled in aqueous 0.02 M Na_2CO_3 for 1 h to remove the sericin proteins and then, the remaining fibroin was thoroughly rinsed three times with distilled water at 70 °C for 20 min each. After dissolving fibroin in aqueous 9.3 M LiBr at 60 °C for 2 h, the solution was poured into dialysis tubes (10000 MWCO, Snake Skin, Pierce) and dialyzed for 3 days against water that was changed three times a day. After centrifugation, the final fibroin concentration was about 5 wt%, as determined by weighing the remaining solid after drying. Aqueous solutions with a higher fibroin concentration were

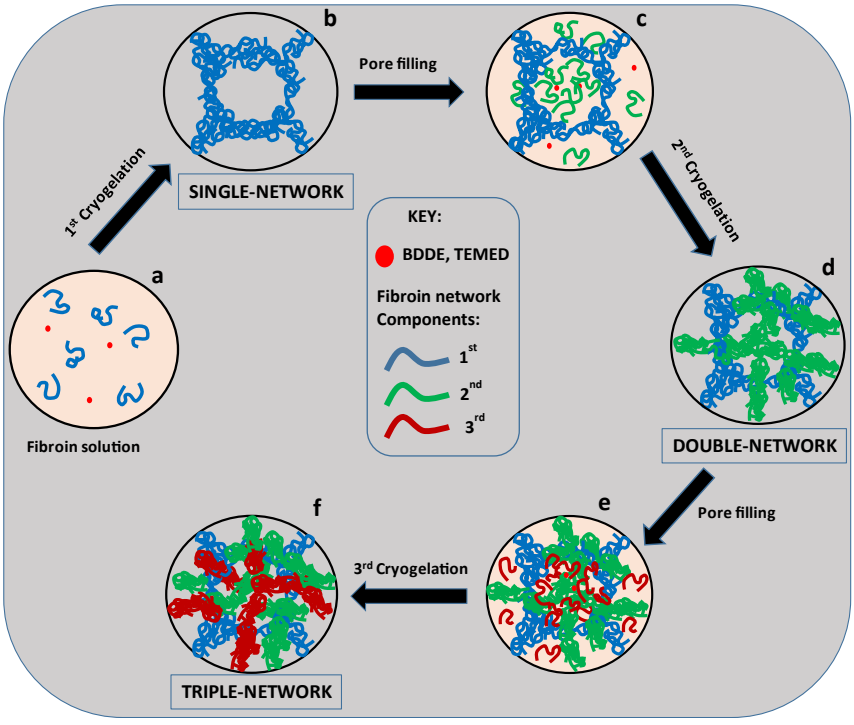

Scheme 1. Cartoon showing the formation of fibroin cryogels with single-, double-, and triple-network structures.

prepared by dialyzing 5 wt% fibroin solution against aqueous solutions of 10 and 15 w/v% poly (ethylene glycol) (PEG, Sigma-Aldrich, molecular weight: ~10000 g mol^{-1}) using 3500 MWCO dialysis tubing (Snake Skin, Pierce). All fibroin solutions were stored at 4 °C and used within 2 weeks.

2.2. Cryogelation reactions

Single-network (SN) fibroin cryogels were prepared at −18 °C in aqueous solutions of various fibroin concentrations C_{SF} between 1 and 61.4 wt% in the presence of BDDE cross-linker and TEMED (0.25 v/v%) as a pH regulator [19,35]. At fibroin concentrations C_{SF} below 15 wt%, BDDE content was fixed at 20 mmol epoxy per gram of fibroin while at higher C_{SF}, the amount of BDDE was reduced to avoid the onset of gelation before the freezing of the reaction solution (Table S1). For instance, at $C_{SF} = 61.4$ wt%, the added amount of BDDE was 1.7 mmol epoxy/g fibroin, which provided a pre-gelation period of 20 min during which the reaction system froze completely. SN cryogels are denoted as SN-*x* where *x* is the nominal fibroin concentration C_{SF} expressed in round number. Typically, to prepare SN-4 cryogels, 5 mL of 5 wt% aqueous fibroin solution were mixed with distilled water (0.49 mL), BDDE (0.50 mL), and TEMED (15 μL), and the reaction solution was transferred into plastic syringes to conduct the cryogelation reactions at-18 °C for 24 h.

Double-network (DN) cryogels were prepared by swelling freeze-dried SN-4 fibroin scaffolds in a 2nd fibroin solution containing BDDE and TEMED, and subsequent cryogelation at −18 °C for 24 h. Fibroin concentration in the 2nd fibroin solution was varied between 7.2 and 28.6 wt% (Table 1). Typically, the extracted and freeze-dried SN-4 cryogel scaffold (about 15 mg) was immersed in 12 mL of 2nd fibroin solution containing BDDE and TEMED. After reaching the swelling equilibrium at 24 ± 2 °C, which required about 90 min, SN cryogel sample swollen in the solution was transferred into plastic syringes of 2.5 mL in volume and the cryogelation was conducted at −18 °C for 24 h.

TN cryogels were prepared similar to DN cryogels by swelling DN cryogels in 20 wt% fibroin solution containing BDDE and TEMED. Preparation conditions of SN, DN, and TN cryogels are tabulated in Table 1 and Table S1. DN and TN cryogels are denoted as DN-*x*/*y* and TN-*x*/*y*/*z* where *x*, *y*, and *z* are the fibroin concentrations in the first, second, and third gelation solutions, respectively, expressed in round numbers.

2.3. Swelling and gel fraction measurements

SN, DN, and TN cryogel samples were immersed in a large excess of water for at least 6 days by replacing water every other day to extract any soluble species. The swelling equilibrium was tested by weighing the gel samples as well as by measuring the diameter of the gel samples by a calibrated digital compass (Mitutoyo Digimatic Caliper, Series 500, resolution: 0.01 mm). The equilibrium swollen gel samples were then frozen at −25 °C for 1 day and freeze-dried using Christ Alpha 2–4 LD-plus freeze-dryer at −40 °C under 0.12 mbar vacuum for 1 day, and at −60 °C under 0.011 mbar for an additional 1 day. The equilibrium weight $q_{w,i}$ and volume swelling ratios $q_{v,i}$, where $i = 1$, 2, and 3 for SN, DN, and TN cryogels, respectively, were calculated as

$$q_{w,i} = \frac{m}{m_{dry}} \tag{1a}$$

$$q_{v,i} = \left(\frac{D}{D_{dry}}\right)^3 \tag{1b}$$

where m and D are the mass and the diameter of the equilibrium swollen gel sample, respectively, and m_{dry} and D_{dry} are the same quantities for the freeze-dried sample. The gel fraction W_g, that is, the conversion of fibroin to the 3D fibroin network (mass of water-insoluble fibroin/initial mass of the fibroin in the feed) was calculated from the masses of dry fibroin network and from the fibroin in the feed.

2.4. Determination of the mass ratio of the network components in DN and TN cryogels

To estimate the mass ratio of the network components in DN cryogels and the nominal fibroin concentration during double-networking, the freeze-dried SN-4 cryogel samples were immersed in aqueous solutions of fibroin of various concentrations and, after equilibrium swelling, the weight swelling ratio $q_{w,1}$ of SN-4 was determined using eq (1a). Fig. 1 shows the swelling ratio $q_{w,1}$ of SN-4 plotted against the fibroin concentration $C_{SF,2}$ in the 2nd fibroin solution. As expected, $q_{w,1}$ decreases with increasing amount of fibroin in the solution due to the osmotic pressure of fibroin molecules in the external solution.

Assuming that the fibroin concentration in the external solution is equal to that in the cryogel, the mass ratio $w_{2/1}$ of the 2nd to the 1st fibroin network components and the total fibroin concentration C_{SF} (in g.g^{-1}) in DN cryogels at their prepared states were estimated as:

$$w_{2/1} = \left(q_{w,1} - 1\right) C_{SF,2} \tag{2a}$$

$$C_{CF} = \frac{1 + w_{2/1}}{q_{w,1}} \tag{2b}$$

Similarly, the mass ratio of 2nd + 3rd to 1st fibroin network components in TNs ($w_{32/1}$), and the total fibroin concentration (C_{SF}) during triple-networking were estimated using the equations:

$$w_{32/1} = w_{2/1} + \left(1 + w_{2/1}\right) w_{3/21} \tag{3a}$$

$$C_{CF} = \frac{1 + w_{3/21}}{q_{w,2}} \tag{3b}$$

where $q_{w,2}$ is the swelling ratio of the DN in the 3rd fibroin solution of concentration $C_{SF,3}$, $w_{3/21}$ is given by $w_{3/21} = (q_{w,2} - 1)C_{SF,3}$, and all concentrations C_{SF} in eqs (2) and (3) are in g.g^{-1}.

2.5. Mechanical tests

Uniaxial compression tests were carried out at 24 ± 2 °C on cryogel specimens both in equilibrium swollen and dried states.

Table 1
Synthesis conditions and characteristics of SN, DN, and TN cryogels. *x*, *y*, and *z* are fibroin concentrations (in wt%) in the 1st, 2nd, and 3rd gelation solutions, respectively. Note that, in the cryogel codes, round numbers of *x*, *y*, and *z* are used. $w_{2/1}$ and $w_{32/1}$ are the mass ratios of the 2nd to 1st and 2nd + 3rd to 1st fibroin network components in the cryogels, respectively. C_{SF} is the nominal fibroin concentration at cryogelation. The numbers in parentheses are standard deviations.

Code	*x* wt%	*y* wt%	*z* wt%	$w_{2/1}$	$w_{32/1}$	C_{SF} wt%
SN-*x*	1 to 61.4	–	–	0	–	1 to 61.4
DN-*x*/*y*	4.2	7.2	–	1.0 (0.1)	–	13.4 (0.5)
		14.3	–	1.7 (0.3)	–	21 (2)
		20.5	–	2.1 (0.2)	–	28 (2)
		28.6	–	2.5 (0.3)	–	36 (7)
TN-*x*/*y*/*z*	4.2	7.2	20	1.0 (0.1)	1.9 (0.2)	45 (3)

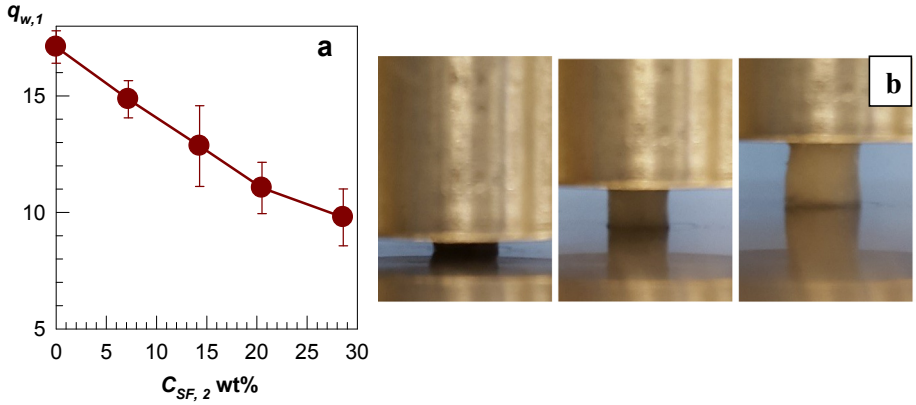

Fig. 1. **(a)** The weight swelling ratio $q_{w,1}$ of SN-4 cryogel in aqueous solutions of fibroin at various concentrations $C_{SF,2}$. **(b)** The optical images of water-swollen SN-4, DN-4/7, and TN-4/7/20 cryogel samples, from left to right, under a force of 1 N. The original dimensions of the gel samples were identical while the strain under 1 N load decreases in the order SN → DN → TN.

The samples were cylindrical in shape with 3.8 ± 0.2 mm in diameter and 4.2 ± 0.5 mm in length. The tests were conducted both on Zwick Roell and Devotrans test machines using 500 N and 10 kN load cells, respectively. An initial compressive contact to 0.1 N (Zwick) or 1 N (Devotrans) was applied to ensure a complete contact between the sample and the surface. Load and displacement data were collected during the experiments at a constant crosshead speed of 0.3 mm min^{-1} (Zwick) or 0.6 mm min^{-1} (Devotrans). Compressive stress was presented by its nominal σ_{nom} and true values σ_{true}, which are the forces per cross-sectional area of the undeformed and deformed specimen, respectively. Assuming constancy of the gel volume during compression, the true stress is related to the nominal stress by $\sigma_{true} = \lambda\ \sigma_{nom}$, where λ is the compression ratio. The compressive strain ε is given by $\varepsilon = 1\text{-}\lambda$, which is the length change of the gel specimen with respect to its initial length. The compression modulus E was calculated from the slope of stress-strain curves between 2 and 4% compressions while the stress at 3% compression was reported as the compressive stress σ_{comp}. For reproducibility, at least six samples were measured for each sample and the results were averaged.

2.6. Texture determination

Scanning electron microscopy measurements of freeze-dried cryogel specimens were conducted at magnifications between 20 and 1000 times on Jeol JSM 6335F Field Emission SEM. Prior to the measurements, the specimens were sputter-coated with gold for 3 min using Sputter-coater S150 B Edwards instrument. Texture determination of the freeze-dried and swollen cryogel specimens was also performed using an image analyzing system consisting of a microscope (XSZ single Zoom microscope), a CDD digital camera (TK 1381 EG) and a PC with the data analyzing system Image-Pro Plus.

2.7. ATR-FTIR measurements

The fibroin conformation in cryogels was investigated by a single bounce diamond attenuated total reflectance (ATR) module on a Fourier-transform infrared (FTIR) spectrometer (Nicolet Nexus 6700) equipped with a liquid nitrogen cooled mercury-cadmium-telluride (MCT) detector. The Spectra were collected at a resolution of 4 cm^{-1}, and 64 interferograms were coadded in the range of 500–4000 cm^{-1}. The conformation of fibroin chains was estimated by analyzing the spectra using PeakFit software (Version 4.12, SeaSolve Software Inc.). Linear baseline correction was applied to the Amide I region (1580–1720 cm^{-1}) before the band was deconvolved by Gauss Amplitude function. For the curve fitting procedure, the initial band positions at 1620, 1640, 1660, and 1698 cm^{-1} representing β-sheet, random coil, α-helix, and β-turn conformations, respectively, were fixed, allowing their widths and heights to vary (Fig. S1) [18,48].

3. Results and discussion

Silk fibroin cryogels were prepared by mixing aqueous fibroin solutions with BDDE cross-linker and TEMED followed by conducting the reactions at −18 °C for 24 h. We previously reported that both the cryogelation temperature and the freezing rate of fibroin solution have significant effects on the morphology of fibroin scaffolds [35]. To eliminate these effects, we fixed the cryogelation temperature (−18 °C) and hence, the freezing rate of fibroin solution throughout this study while only the nominal fibroin concentration was varied. As detailed above, we prepared two series of fibroin cryogels:

a) Single-network (SN) cryogels: By varying the nominal fibroin concentration C_{SF} in the gelation solution between 1 and 61 wt%, twenty-two cryogel samples with a single-network structure were obtained (Table S1).
b) Double-network (DN) and triple-network (TN) cryogels: Freeze-dried SN-4 cryogels were immersed in an excess of aqueous fibroin solution containing BDDE and TEMED. After pore-filling with the solution, the cryogelation reactions were conducted at −18 °C for 24 h to obtain DN cryogels (Scheme 1). In a similar way, TN cryogels were prepared by first swelling freeze-dried DN-4/7 cryogels in aqueous solutions of fibroin, BDDE, and TEMED, followed by cryogelation at −18 °C for 24 h.

Because both double- and triple-networking increase the fibroin content of the cryogels in a manner similar to increasing fibroin concentration during the preparation of SNs, we compare the results of the experiments by taking fibroin concentration C_{SF} of cryogels as the independent variable, while the type of fibroin network (SN, DN, or TN) is indicated in the figures. In the following, we discuss the results of our experiments in two subsections. In the first subsection, swelling characteristics and morphologies of SN, DN, and TN cryogels are compared. In the second subsection, the mechanical properties are discussed, and experimental observations are interpreted.

3.1. Swelling behavior and morphology of cryogels

Fig. 2a shows the gel fraction W_g of fibroin cryogels with SN (circles), DN (triangles up), and TN structures (triangle down) plotted against the fibroin concentration C_{SF}. The gel fraction W_g of SN cryogels is close to unity up to C_{SF} = ~30 wt% indicating that all fibroin molecules in the feed are incorporated into the 3D fibroin network, while at higher fibroin concentrations W_g decreases probably due to the steric effect hindering gelation reactions (Table S1). Note that the values of W_g above unity measured at low fibroin concentrations suggest the presence of bound water that cannot be removed from the fibroin network during drying. DN and TN cryogels also exhibit a complete gel fraction revealing that the second and third network components cannot be extracted from the cryogels (Table S1).

As previously reported, fibroin gelation via diepoxide cross-linkers occurs due to the formation of intermolecular β-sheet structures between fibroin molecules [19]. Although a conformational transition in fibroin molecules from random coil to β-sheet structures is slow and even slower at lower temperatures, this transition is accelerated by the presence of diepoxide cross-linkers. Introduction of BDDE cross-links between fibroin molecules reduces the mobility of the molecules by connecting them together, which triggers the conformational transition from random-coil to β-sheet structure and hence fibroin gelation [19]. FTIR measurements showed that the β-sheet content of fibroin is 12 ± 2% before gelation while it increases to 36 ± 7% in all cryogel scaffolds reported in this study (see: Table S1, Fig. S1, and the related text). Increasing fibroin concentration from 4.2 to 61.4 wt% or applying the double- and triple-networking procedures did not affect the β-sheet content of the cryogels. Moreover, complete gel fraction of DN and TN cryogels together with their high β-sheet contents suggest that the individual network components are interconnected via β-sheet crystallites acting as grafting points.

Swelling behavior of the cryogels was investigated by immersing cryogel samples into an excess of water and monitoring the mass and volume changes. Fig. 2b presents the equilibrium weight $q_{w,i}$ and volume swelling ratios $q_{v,i}$ of SN (circles), DN (triangles up), and TN cryogels (triangle down) as a function of fibroin concentration C_{SF}. It is seen that C_{SF} is the only parameter determining the swelling behavior of single- and multiple-network cryogels, indicating that the double- or triple-networking have no other effect than to increase the fibroin content of the cryogel. The volume swelling ratio $q_{v,i}$ is independent on the fibroin concentration C_{SF} and is close to unity (1.1 ± 0.2) over the whole range of C_{SF}, revealing that the volume of the cryogels does not change much after their swelling in water. The slightly larger value of $q_{v,i}$ from unity is attributed to the absorption of bound water by fibroin molecules [49]. In contrast, the weight swelling ratio $q_{w,i}$ strongly depends on the fibroin concentration C_{SF} and it decreases from 35 to 4 on rising C_{SF} from 1 to 30 w/v%.

The large difference between the weight $q_{w,i}$ and volume swelling ratios $q_{v,i}$ as well as the equality of $q_{v,i}$ close to unity reveal that the swelling of fibroin cryogels mainly occurs by filling their pores with water. This is due to the fact that the filling of the pores with water will not increase the cryogel volume while its mass will increase proportionally with the pore volume. Because the pores are generated from the ice crystals acting as template during cryogelation, the lower the fibroin concentration C_{SF}, the larger is the total volume of ice and hence the larger is both the porosity and the weight swelling ratio. Thus, the weight swelling ratio $q_{w,i}$ and the total porosity P (total volume of open pores/volume of the polymer) can be estimated using the equations [50]:

$$q_{w,i} = \left(C_{SF} W_g\right)^{-1} \tag{4}$$

$$P = 1 - q_{v,i}\left[1 + \left(q_{w,i} - 1\right)\rho\right]^{-1} \tag{5}$$

where ρ is the fibroin density (1.35 g/mL). According to eqs (4) and (5), increase in C_{SF} decreases both $q_{w,i}$ and P. The solid curve in Fig. 2b calculated using eq (4) indicates that it well reproduces the observed swelling behavior of the cryogels. The porosity P of all cryogels calculated using eq (5) are collected in Fig. 2c. It is seen that they all exhibit 97% porosity at low fibroin concentration while the porosity decreases with increasing C_{SF} and approaches to 70% at high fibroin concentration.

In accord with the swelling results, optical and SEM images visualized highly porous structure of the cryogel scaffolds (Fig. S2, S3). Fig. 3 shows SEM images of SNs formed at fibroin concentrations C_{SF} between 4.2 and 46.2 wt%, as indicated on the images. All scaffolds possess macropores that are circular and rectangular in shapes within an interconnected fibroin network. The diameter of the pores decreases while the thickness of the pore wall increases as the fibroin concentration C_{SF} is increased. For instance, the average pore diameter decreases from 30 ± 7 to 9 ± 4 μm while the wall thickness increases from <1.5 μm to 2–13 μm as C_{SF} is increased from 4.2 to 39 wt%. Because an increase in C_{SF} means a decrease in the total volume of ice present during cryogelation,

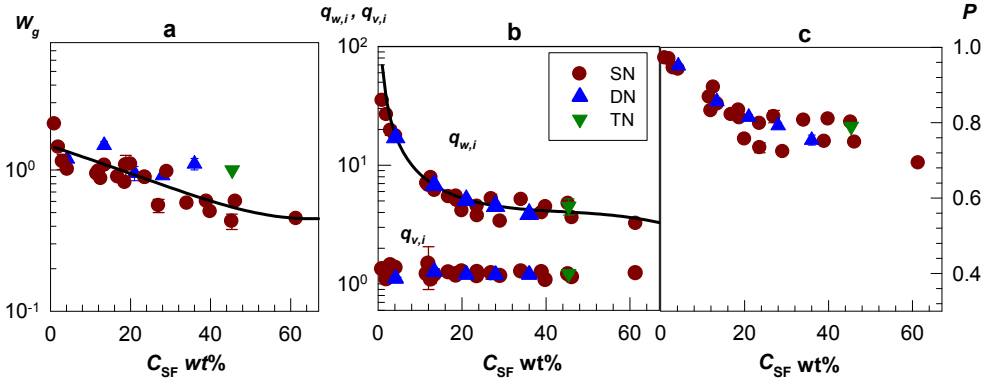

Fig. 2. **(a)** The gel fraction W_g of fibroin cryogels with SN (circles), DN (triangles up) and TN structures (triangle down) plotted against the fibroin concentration C_{SF}. The curve is the best fit to the data points yielding the equation $W_g = y_0 + aC_{SF}\% + bC_{SF}\%^2$, where $y_0 = 1.5 \pm 0.1$, $a = -3.2 \pm 0.9 \times 10^{-2}$, and $b = 2.4 \pm 1.6 \times 10^{-4}$. **(b)** The weight $q_{w,i}$ and volume swelling ratios $q_{v,i}$ of SN, DN, and TN cryogels shown as a function of C_{SF}. The curve was calculated using eq (4) together with W_g equation given above. **(c)** Porosities P of SN, DN, and TN cryogels calculated using eq (5) plotted against C_{SF}.

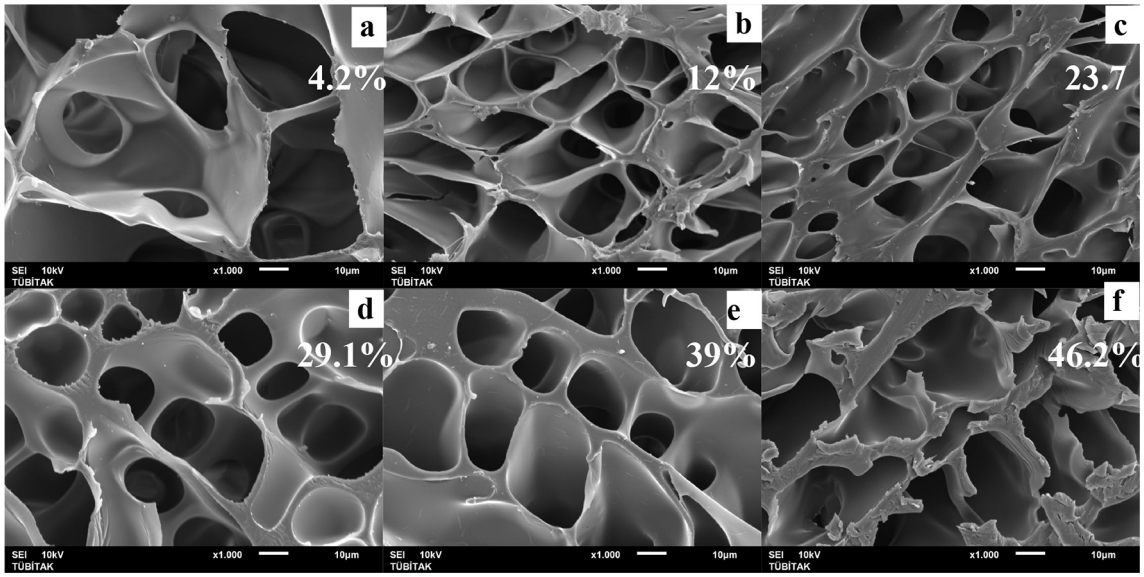

Fig. 3. SEM images of SN fibroin scaffolds prepared at fibroin concentrations indicated. Scaling bars = 10 μm (Magnification = ×1000). The codes of the cryogels: SN-4 (a), SN-12 (b), SN-24 (c), SN-29 (d), SN-39 (e), and SN-46 (f).

fibroin scaffolds with smaller pores separated by thicker pore walls form at high fibroin concentrations. The pore walls approaching to 13 μm in thickness at high fibroin concentrations are remarkable and originate from highly cryo-concentrated fibroin in unfrozen domains building the pore walls.

Fig. 4 compares SEM images of the double-network DN-4/14 scaffold (left panel) with its precursor single-network SN-4 (right panel) at two different magnifications. In contrast to the morphology of the SN, DN exhibits two generations of μm-sized pores. The large pores existing in SN-4 slightly decrease in size after double-networking, and simultaneously additional small pores appear within the large pores. The images at a smaller magnification shown in the upper panel of Fig. 4 also reveal that the interconnected pore structure of the initial SN remains preserved in the resulting DN scaffold. Fig. 5 shows SEM images of the triple-network TN-4/7/20 scaffold together with its two precursors, namely DN-4/7 and SN-4. The large pores become smaller after double- and subsequent triple-networking of the initial SN due to the gradual filling of the pores with successive fibroin networks. Moreover, the small pores of 8 ± 1 μm in diameter appeared after

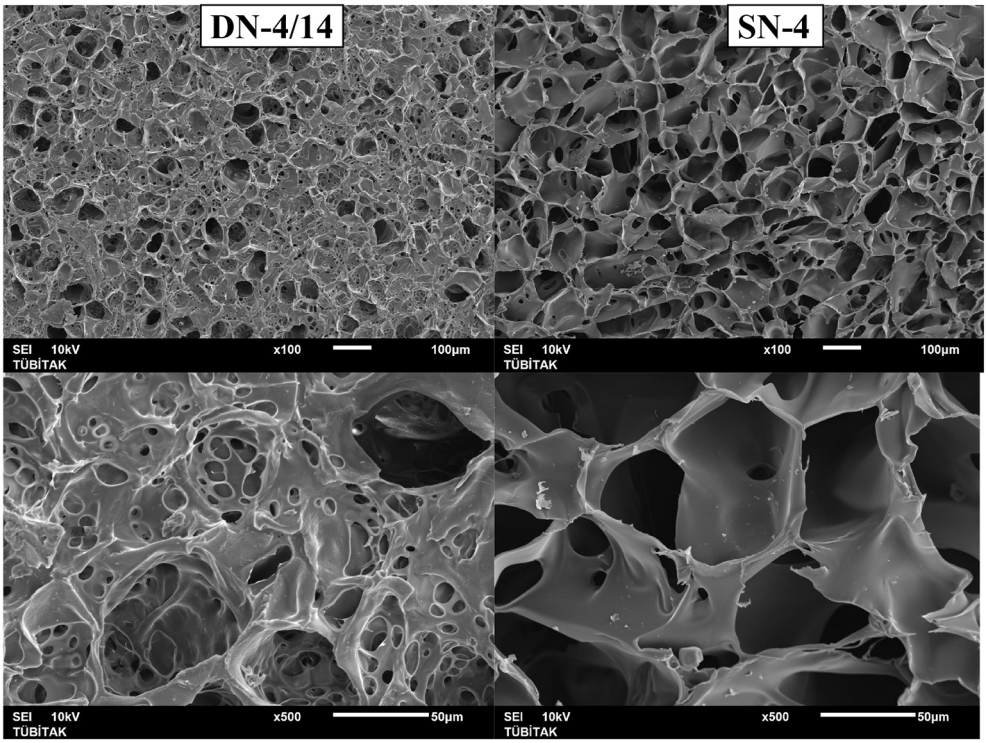

Fig. 4. SEM images of DN-4/14 (left panel) and its precursor SN-4 fibroin scaffolds (right panel). Scaling bars = 100 (up) and 50 μm (down) (Magnification = ×100 and ×500).

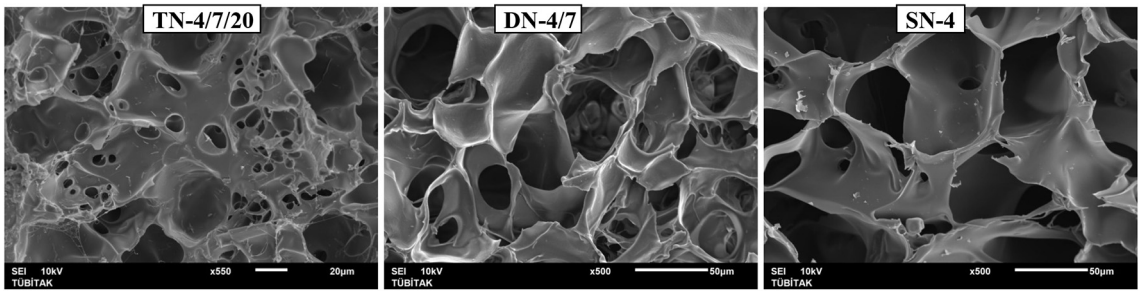

Fig. 5. SEM images of SN-4, DN-4/7, and TN-4/7/20 fibroin scaffolds. Scaling bars = 20 μm (TN) and 50 μm (DN and SN).

double-networking of SN-4 also decreases in size to 2 ± 1 μm diameter after triple-networking of DN-4/7.

The average diameter of large pores in SN, DN, and TN scaffolds is presented in Fig. 6a by the filled symbols as a function of the fibroin concentration C_{SF}. The large error bars are due to the large distribution of pore diameters. Independent of the type of the network structure, all scaffolds having the same fibroin concentration C_{SF} possess similar diameters of large pores that are decreasing from ~30 μm to ~10 μm with increasing C_{SF} from 4 to 61 wt%. However, the thickness of pore walls in SN significantly increases from <1.5 μm up to 13 μm with increasing C_{SF} while it only slightly increases after double- and triple-networking, i.e., from 1.5 ± 0.5 μm (DN-4/7) to 2.7 ± 1.5 μm (DN-4/29), and 6 ± 2 μm (TN-4/7/20). This is reasonable considering the fact that all fibroin molecules present during single-networking forms the walls of the large pores while, during double- and triple-networking, they are consumed to create the walls of the additional smaller pores. Open symbols in Fig. 6a representing the pore diameters in swollen SN cryogels measured using image analyzing system reveal that the pores do not change their size after swelling, as expected from the equality of the volume swelling ratio $q_{v,i}$ of the cryogels close to unity (Fig. 2b).

In Fig. 6b, the average diameter of large and small pores is plotted against the mass ratio $w_{2/1}$ of the 2nd to the 1st network components in DN cryogels. Note that the data at $w_{2/1} = 0$ corresponds to the single-network SN-4 scaffold having only large pores of 30 ± 7 μm in diameter. Increasing $w_{2/1}$ ratio decreases the diameter of large pores and simultaneously, a second generation of small pores appears. The small pores are monodisperse in size as compared to larger ones (Fig. 6a) and their diameter decreases from 9 ± 2 to 5 ± 2 μm with increasing $w_{2/1}$ ratio. The triangles in Fig. 6b present the average diameter of large and small pores in the triple-network TN-4/7/20 formed at $w_{2/1} = 1.0$ and $w_{32/1} = 1.9$. As compared to its precursor DN-4/7, the diameter of small pores further decreases from 9 ± 2 to 3.4 ± 1.5 μm after triple-networking. Thus, the diameters of both large and small pores can be adjusted by varying the amount of fibroin in the 2nd and 3rd network components.

3.2. Mechanical properties

Even visual observations revealed a significant increase in the stiffness of the cryogels after formation of double- and triple-networks. For instance, the images in Fig. 1b represent water-swollen SN-4, DN4/7, and TN-4/7/20 cryogel samples, from left to right, each under a load of 1 N. Although their original dimensions are identical, the strain decreases in the order of SN→DN→TN indicating increasing resistance to deformation.

Mechanical properties of fibroin cryogels were quantified by uniaxial compression tests. In Fig. 7a and b, stress-strain curves of the precursor SN, denoted by $w_{2/1} = 0$, and resulting DNs in their dry states are shown, where the nominal σ_{nom} and trues stresses σ_{true} are plotted against the compressive strain ε. The mass ratio $w_{2/1}$ of the 2nd to the 1st network components in the DNs are indicated. DN cryogels sustain up to about 400 MPa nominal stresses at 95% compression. However, converting the nominal stress to its

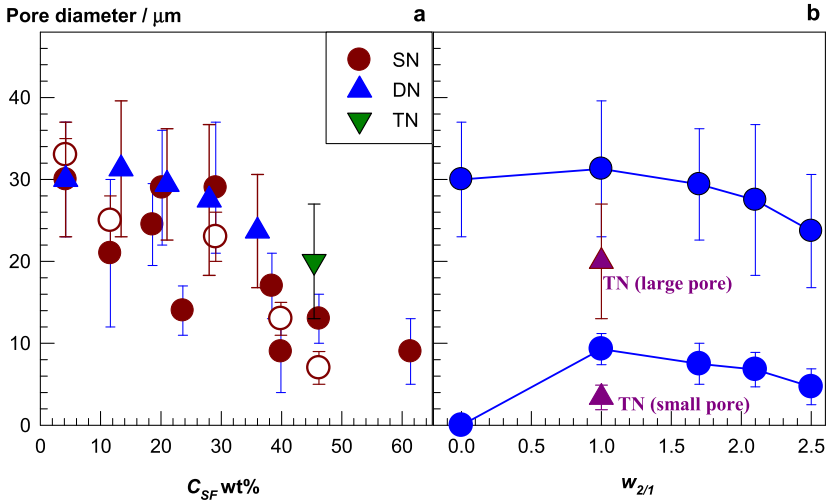

Fig. 6. **(a)** Average pore diameter of SN, DN, and TN cryogel scaffolds plotted against the fibroin concentration C_{SF}. The open symbols represent pore diameters in swollen SN cryogels. **(b)** Average pore diameters of large and small pores plotted against the mass ratio $w_{2/1}$ of the 2nd to the 1st network components in DN cryogels. The triangles represent the data for the triple-network TN-4/7/20 ($w_{2/1} = 1.0$, $w_{32/1} = 1.9$) derived from SN-4 and DN-4/7 precursors.

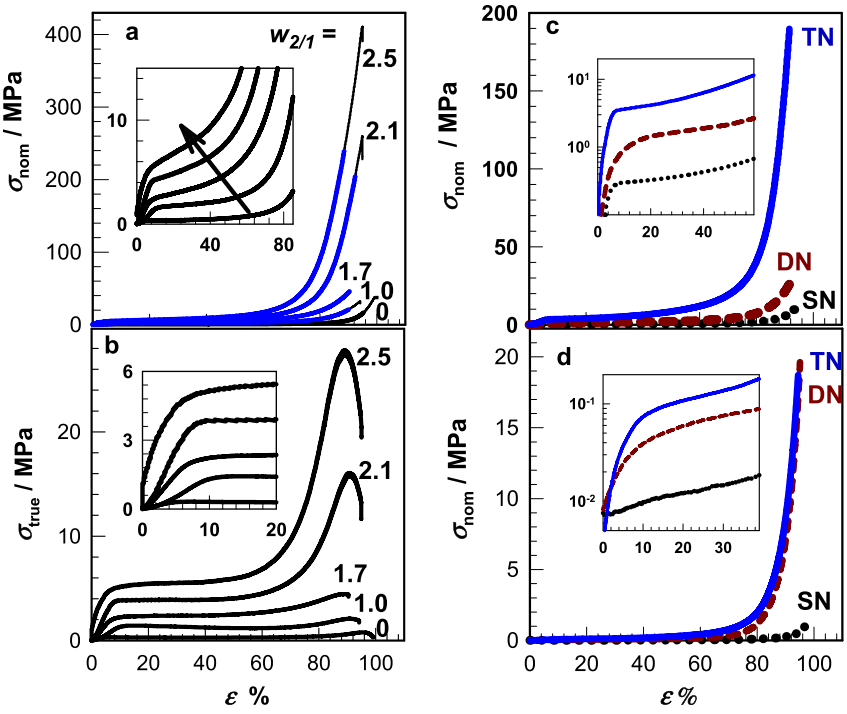

Fig. 7. **(a, b)** Stress – strain curves of SN and DN fibroin scaffolds as the dependence of the nominal σ_{nom} and true stresses σ_{true} on the compressive strain ε. The mass ratio $w_{2/1}$ of the 2nd to the 1st network components in the cryogels are indicated. **(c, d)** The dependence of σ_{nom} on ε for SN-4, DN-4/7, and TN-4/7/20 cryogels in dry (c) and swollen states (d). The codes are abbreviated in the figures as SN, DN, and TN, respectively. The insets are semi-logarithmic plots up to the strain of 40–50%.

true value and plotting the trues stress σ_{true} against deformation, the resulting stress-strain curves exhibit maxima at lower compressions (Fig. 7b). This indicates the occurrence of a microscopic crack in the cryogels that cannot be detected in the nominal stress-strain curves [51,52]. Therefore, σ_{nom}–ε curves were corrected by drawing up to the maximum point in σ_{true}–ε plots as shown by the blue bold curves in Fig. 7a. The corrected stress-strain curves reveal that increasing amount of fibroin in the second network significantly improves the mechanical properties of the cryogels. Cryogels formed at $w_{2/1}$ = 2.5 sustain 240 ± 24 MPa stress at 88% compression (Table S2). Moreover, the single-network SN-4 cryogel with $w_{2/1}$ = 0 does not support a high load and the work of deformation, i.e., the area under the stress-strain curve up to the fracture point is 1.4 MJ m^{-3}. Double-networking at a level of $w_{2/1}$ = 1.7 and 2.5 increases the work of deformation to 7.5 and 26.4 MJ m^{-3}, respectively, which are 5- and 19-fold larger than that of the precursor SN-4.

The inset to Fig. 7a which is a zoom-in to the compressive stresses of below 15 MPa reveals the appearance of a near-plateau regime starting from 5% compression. This regime can also be seen in σ_{true}–ε plots of Fig. 7b. We attribute this plateau to the onset of collapse of the porous structure so that the samples easily deform under force. Increasing plateau stress with increasing $w_{2/1}$ ratio indicates increasing mechanical stability of the porous structure in the cryogels. Fig. 7c and d shows stress-strain curves of the triple-network TN-4/7/20 in dry and swollen states, respectively, together with its precursors DN-4/7 and SN-4. All the curves were corrected up to the maxima in σ_{true}–ε plots. The insets show the plots in a semi-logarithmic scale up to the strain of 40–50%. Both double- and triple-networking significantly improve the mechanical properties of both dry and swollen cryogels (Table S2). For instance, after triple-networking, the work of deformation of dry and swollen SN cryogels increases by a factor of 13 and 19, and become 18.5 and 1.3 MJ m^{-3}, respectively.

Fig. 8 and Table S2 show the Young's modulus E, fracture stress σ_f, compressive stress σ_{comp}, and plateau stress $\sigma_{plateau}$ of swollen (open symbols) and dried SN, DN, and TN cryogels (filled symbols) as a function of the fibroin concentration C_{SF}. Comparison of the mechanical properties of DN and TN cryogels with SNs reveals that the improvement in the mechanical properties of cryogels after multiple-networking is due to their increased content of fibroin network. That is, SN, DN, and TNs having the same fibroin content exhibit similar mechanical properties. Thus, multiple-networking creates small pores in cryogels in addition to larger ones without deteriorating their mechanical properties. The modulus E of fibroin scaffolds varies between 10^1 and 10^2 MPa with a largest modulus of 126 ± 2 MPa obtained at C_{SF} = 46 wt%. Moreover, all the scaffolds formed above C_{SF} = 25 wt% sustain compressive stresses of 87–240 MPa. The plateau stress also increases with fibroin concentration indicating increasing stability of the porous structure.

The results in Fig. 8 also show that the modulus, compressive and plateau stresses of the cryogels decrease by one order of magnitude after swelling in water. However, even in swollen states, cryogels prepared at fibroin concentrations above 20 wt% exhibit a modulus in the range of MPa. For instance, swollen cryogels formed between C_{SF} = 20 and 38.3 wt% have a modulus E of 1.25–2.5 MPa (Table S2), which is comparable to the modulus of 1.23 MPa reported for the human intervertebral disc tissue [53]. Because swollen cryogels mainly contain free water in their pores, the bound water seems to be responsible for the reduction in the mechanical properties of swollen cryogels. It has been reported that around 5% of bound water exist in fibroin molecules acting as a plasticizer to induce glassy to rubbery transition [49]. The volume swelling ratio $q_{v,i}$ of 1.1 ± 0.2 of fibroin cryogels corresponding to a water absorption of 10% can thus be accounted for the water bound to fibroin molecules. We have to note that DN cryogels based on synthetic polymers have recently been reported by Zhao et al. [45]. The Young's modulus of these cryogels in their swollen states is

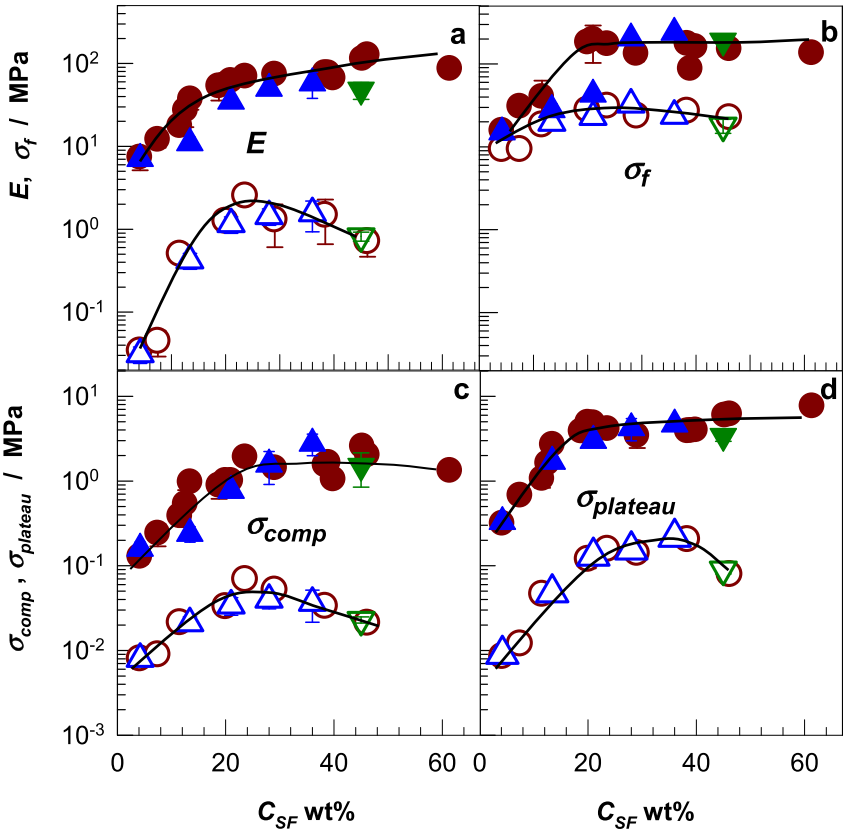

Fig. 8. The compressive modulus E (a), fracture stress σ_f (b), compressive stress σ_{comp} (c), and plateau stress $\sigma_{plateau}$ (d) of SN (circles), DN (triangles up), and TN cryogels (triangles down) in dry (filled symbols) and swollen states (open symbols) shown as a function of C_{SF}. Curves show the trend of data.

below 52 kPa, which is 30- and 50-fold smaller than swollen SN-24 and DN-4/29 fibroin cryogels (2.53 ± 0.02 and 1.6 ± 0.6 MPa, Fig. 8, Table S2). Because the cryogelation reactions in Ref. [45] were conducted at −8 °C, the possible onset of gelation prior to freezing of the reaction system can be responsible for the low mechanical strength.

4. Conclusions

Mechanically strong silk fibroin cryogels with two generation of pores were produced from fibroin solutions frozen at −18 °C in the presence of BDDE cross-linker and TEMED as a pH regulator. To obtain multiple-network structures, the cryogelation reactions were carried out within the pores of the precursor cryogels. The water insolubility of all scaffolds suggests formation of interpenetrated and interconnected network structures. Cryogel scaffolds formed at fibroin concentrations above 25 wt% exhibit a Young's modulus between 66 and 126 MPa that sustain around 90% compressions under 87–240 MPa stresses. These values are the largest reported so far for fibroin scaffolds. Moreover, because fibroin scaffolds formed in aqueous media completely degrade between two and six months [54], mechanically strong SN, DN, and TN fibroin scaffolds have promising applications in bone tissue engineering. Both DN and TN cryogels have two generations of interconnected macropores with diameters 20–30 μm and 3–9 μm. The size of both large and small pores could be adjusted by the relative amounts of fibroin in the network components. Comparison of the swelling and mechanical properties of SN cryogels with the DN and TN ones reveals that they all exhibit similar swelling and mechanical characteristics as long as their fibroin concentrations are equal. Thus, multiple-networking creates small pores in fibroin cryogels in addition to the larger ones without deteriorating their mechanical properties.

Acknowledgments

Work was supported by the Scientific and Technical Research Council of Turkey (TUBITAK), KBAG 114Z312, and Istanbul Technical University, BAP 39957. O.O. thanks the Turkish Academy of Sciences (TUBA) for the partial support.

Appendix A. Supplementary data

Supplementary data related to this article can be found at http://dx.doi.org/10.1016/j.polymer.2017.09.023.

References

[1] C. Vepari, D.L. Kaplan, Silk as a biomaterial, Prog. Polym. Sci. 32 (2007) 991–1007.
[2] F. Vollrath, D. Porter, Silks as ancient models for modern polymers, Polymer 50 (2009) 5623–5632.
[3] J.G. Hardy, L.M. Romer, T.R. Scheibel, Polymeric materials based on silk proteins, Polymer 49 (2008) 4309–4327.
[4] J. Melke, S. Midha, S. Ghosh, K. Ito, S. Hofmann, Silk fibroin as biomaterial for bone tissue engineering, Acta Biomater. 31 (2016) 1–16.
[5] C.Z. Zhou, F. Confalonieri, N. Medina, Y. Zivanovic, C. Esnault, T. Yang, M. Jacquet, J. Janin, M. Duguet, R. Perasso, Z.G. Li, Fine organization of Bombyx mori fibroin heavy chain gene, Nucleic Acids Res. 28 (2000) 2413–2419.
[6] H.J. Jin, D.L. Kaplan, Mechanism of silk processing in insects and spiders, Nature 424 (2003) 1057–1061.
[7] U.J. Kim, J. Park, C. Li, H.J. Jin, R. Valluzzi, D.L. Kaplan, Structure and properties of silk hydrogels, Biomacromolecules 5 (2004) 786–792.
[8] A. Matsumoto, J. Chen, A.L. Collette, U.J. Kim, G.H. Altman, P. Cebe, D.L. Kaplan, Mechanisms of silk fibroin sol-gel transitions, J. Phys. Chem. B 110 (2006) 21630–21638.

[9] J. Magoshi, Y. Magoshi, S. Nakamura, Mechanism of fiber formation of silkworm, in: D. Kaplan, W.W. Adams, B. Farmer, C. Viney, C (Eds.), Silk Polymers, American Chemical Society, Washington, 1994, pp. 292–310.
[10] A. Matsumoto, A. Lindsay, B. Abedian, D.L. Kaplan, Silk fibroin solution properties related to assembly and structure, Macromol. Biosci. 8 (2008) 1006–1018.
[11] X. Chen, D.P. Knight, F. Vollrath, Rheological characterization of Nephila Spidroin solution, Biomacromolecules 3 (2002) 644–648.
[12] A.E. Terry, D.P. Knight, D. Porter, F. Vollrath, pH induced changes in the rheology of silk fibroin solution from the middle division of Bombyx mori silkworm, Biomacromolecules 5 (2004) 768–772.
[13] C. Dicko, F. Vollrath, J.M. Kenney, Spider silk protein refolding is controlled by changing pH, Biomacromolecules 5 (2004) 704–710.
[14] X.H. Zong, P. Zhou, Z.Z. Shao, S.M. Chen, X. Chen, B.W. Hu, F. Deng, W.H. Yao, Effect of pH and copper(II) on the conformation transitions of silk fibroin based on EPR, NMR, and Raman spectroscopy, Biochemistry 43 (2004) 11932–11941.
[15] C. Dicko, J.M. Kenney, D. Knight, F. Vollrath, Transition to a beta-sheet-rich structure in spidroin in vitro: the effects of pH and cations, Biochemistry 43 (2004) 14080–14087.
[16] A. Ochi, K.S. Hossain, J. Magoshi, N. Nemoto, Rheology and dynamic light scattering of silk fibroin solution extracted from the middle division of Bombyx mori silkworm, Biomacromolecules 3 (2002) 1187–1196.
[17] K.S. Hossain, A. Ochi, J. Magoshi, N. Nemoto, Dynamic light scattering of native silk fibroin solution extracted from different parts of the middle division of the silk gland of the Bombyx mori silkworm, Biomacromolecules 4 (2003) 350–359.
[18] X. Chen, D.P. Knight, Z.Z. Shao, F. Vollrath, Conformation transition in silk protein films monitored by time-resolved Fourier transform infrared spectroscopy: effect of potassium ions on Nephila spidroin films, Biochemistry 41 (2002) 14944–14950.
[19] I. Karakutuk, F. Ak, O. Okay, Diepoxide-triggered conformational transition of silk fibroin: formation of hydrogels, Biomacromolecules 13 (2012) 1122–1128.
[20] T. Yucel, P. Cebe, D.L. Kaplan, Vortex-induced injectable silk fibroin hydrogels, Biophys. J. 97 (2009) 2044–2050.
[21] E. Servoli, D. Maniglio, A. Motta, C. Migliaresi, Folding and assembly of fibroin driven by an AC electric field: effects on film properties, Macromol. Biosci. 8 (2008) 827–835.
[22] G.G. Leisk, T.J. Lo, T. Yucel, Q. Lu, D.L. Kaplan, Electrogelation for protein adhesives, Adv. Mater 22 (2010) 711–715.
[23] T. Yucel, N. Kojic, G.G. Leisk, T.J. Lo, D.L. Kaplan, Non-equilibrium silk fibroin adhesives, J. Struct. Biol. 170 (2010) 406–412.
[24] V. Karageorgiou, D.L. Kaplan, Porosity of 3D biomaterial scaffolds and osteogenesis, Biomaterials 26 (2005) 54745491.
[25] R. Nazarov, H.J. Jin, D.L. Kaplan, Porous 3-D scaffolds from regenerated silk fibroin, Biomacromolecules 5 (2004) 718–726.
[26] C.S. Ki, S.Y. Park, H.J. Kim, H.M. Jung, K.M. Woo, J.W. Lee, Y.H. Park, Development of 3-D nanofibrous fibroin scaffold with high porosity by electrospinning: implications for bone regeneration, Biotechnol. Lett. 30 (2008) 405–410.
[27] D.W. Hutmacher, Scaffolds in tissue engineering bone and cartilage, Biomaterials 21 (2000) 2529–2543.
[28] M.Z. Li, S.Z. Lu, Z.Y. Wu, H.J. Yan, Study on porous silk fibroin materials. I. Fine structure of freeze dried silk fibroin, J. Appl. Polym. Sci. 79 (2001) 2185–2191.
[29] Z. Cao, J. Wen, J. Yao, X. Chen, Y. Ni, Z. Shao, Facile fabrication of the porous three-dimensional regenerated silk fibroin scaffolds, Mater. Sci. Eng. C33 (2013) 3522–3529.
[30] Q. Lv, Q.L. Feng, Preparation of 3-D regenerated fibroin scaffolds with freeze drying method and freeze drying/foaming technique, J. Mater. Sci. Mater. Med. 17 (2006) 1349–1356.
[31] X. Liu, P.X. Ma, Polymeric scaffolds for bone tissue engineering, Ann. Biomed. Eng. 32 (2004) 477–486.
[32] Q. Zhang, S. Yan, M. Li, Silk fibroin based porous materials, Materials 2 (2009) 2276–2295.
[33] U.J. Kim, J. Park, H.J. Kim, M. Wada, D.L. Kaplan, Three-dimensional aqueous-derived biomaterial scaffolds from silk fibroin, Biomaterials 26 (2005) 2775–2785.
[34] S. Min, X. Gao, L. Liu, L. Tian, L. Zhu, H. Zhang, J. Yao, Fabrication and characterization of porous tubular silk fibroin scaffolds, J. Biomater. Sci. 20 (2009) 1961–1974.
[35] F. Ak, Z. Oztoprak, I. Karakutuk, O. Okay, Macroporous silk fibroin cryogels, Biomacromolecules 14 (2013) 719–727.
[36] K.R. Hixon, C.T. Eberlin, P.U. Kadakia, S.H. McBride-Gagyi, E. Jain, S.S. Sell, A comparison of cryogel scaffolds to identify an appropriate structure for promoting bone regeneration, Biomed. Phys. Eng. Express 2 (2016) 035014.
[37] V.I. Lozinsky, Cryogels on the basis of natural and synthetic polymers: preparation, properties and application, Russ. Chem. Rev. 71 (2002) 489–511.
[38] O. Okay, V.I. Lozinsky, Synthesis and structure–property relationships of cryogels, Adv. Polym. Sci. 263 (2014) 103–157.
[39] V.I. Lozinsky, O. Okay, Basic principles of cryotropic gelation, Adv. Polym. Sci. 263 (2014) 49–101.
[40] R.K. Singh, G.Z. Jin, C. Mahapatra, K.D. Patel, W. Chrzanowski, H.-W. Kim, Mesoporous silica-layered biopolymer hybrid nanofibrous scaffold: a novel nanobiomatrix platform for therapeutics delivery and bone regeneration, ACS Appl. Mater. Interf. 7 (2015) 8088–8098.
[41] T. Lou, X. Wang, G. Song, Z. Gu, Z. Yang, Fabrication of PLLA/beta-TCP nanocomposite scaffolds with hierarchical porosity for bone tissue engineering, Int. J. Biol. Macromol. 69 (2014) 464–470.
[42] G. Xiong, H. Luo, Y. Zhu, S. Raman, Y. Wan, Creation of macropores in three-dimensional bacterial cellulose scaffold for potential cancer cell culture, Carbohydr. Polym. 114 (2014) 553–557.
[43] T. Wang, Z.-Q. Feng, M.K. Leach, J. Wu, Q. Jiang, Nanoporous fibers of type-I collagen coated poly(l-lactic acid) for enhancing primary hepatocyte growth and function, J. Mater. Chem. B 1 (2013) 339–346.
[44] X. Wang, T. Lou, W. Zhao, G. Song, C. Li, G. Cui, The effect of fiber size and pore size on cell proliferation and infiltration in PLLA scaffolds on bone tissue engineering, J. Biomater. Appl. 30 (2016) 1545–1551.
[45] Q. Zhao, J. Sun, X. Wu, Y. Lin, Macroporous double-network cryogels: formation mechanism, enhanced mechanical strength and temperature/pH dual sensitivity, Soft Matter 7 (2011) 4284–4293.
[46] J.P. Gong, Y. Katsuyama, T. Kurokawa, Y. Osada, Double-network hydrogels with extremely high mechanical strength, Adv. Mater 15 (2003) 1155–1158.
[47] Y. Tanaka, R. Kuwabara, Y.-H. Na, T. Kurokawa, J.P. Gong, Y. Osada, Determination of fracture energy of high strength double network hydrogels, J. Phys. Chem. B 109 (2005) 11559–11562.
[48] C. Mo, C. Holland, D. Porter, Z. Shao, F. Vollrath, Concentration state dependence of the rheological and structural properties of reconstituted silk, Biomacromolecules 10 (2009) 2724–2728.
[49] X. Hua, D. Kaplan, P. Cebe, Effect of water on the thermal properties of silk fibroin, Thermochim. Acta 461 (2007) 137–144.
[50] O. Okay, Macroporous copolymer networks, Prog. Polym. Sci. 25 (2000) 711–779.
[51] A. Argun, V. Can, U. Altun, O. Okay, Non-ionic double and triple network hydrogels of high mechanical strength, Macromolecules 47 (2014) 6430–6440.
[52] B. Tavsanli, V. Can, O. Okay, Mechanically strong triple network hydrogels based on hyaluronan and poly(N,N-dimethylacrylamide), Soft Matter 11 (2015) 8517–8524.
[53] Y. Schroeder, D.M. Elliott, W. Wilson, F.P.T. Baaijens, J.M. Huyghe, Experimental and model determination of human intervertebral disc osmoviscoelasticity, J. Orthop. Res. 26 (2008) 1141–1146.
[54] Y. Wang, D.D. Rudym, A. Walsh, L. Abrahamsen, H.-J. Kim, H.S. Kim, C. Kirker-Head, D.L. Kaplan, In vivo degradation of three-dimensional silk fibroin scaffolds, Biomaterials 29 (2008) 3415–3428.